Urchin-inspired ZnO-TiO 2 core-shell as building blocks for dye sensitized solar cells

Chantal Karam, Carlos Guerra-Nuñez, Roland Habchi, Ziad Herro, Nadine Abboud, Antonio Khoury, Sophie Tingry, Philippe Miele, Ivo Utke, Mikhael Bechelany

Urchin-Inspired ZnO-TiO_2 Core-Shell as Building Blocks for Dye Sensitized Solar Cells

Chantal Karam[a,b 1], *Carlos Guerra-Nuñez*[c,1], *Roland Habchi*[d], *Ziad Herro*[b], *Nadine Abboud*[b], *Antonio Khoury*[b], *Sophie Tingry*[a], *Philippe Miele*[a], *Ivo Utke*[c*], *Mikhael Bechelany*[a*]

[a]European Institute of Membranes (IEM ENSCM UM CNRS UMR 5635), University of Montpellier, Place Eugene Bataillon, 34095 Montpellier, France

[b]Applied Physics Laboratory, Lebanese University, Faculty of Sciences 2, BP 90656 Jdeidet, Lebanon.

[c]EMPA, Swiss Laboratories for Materials Science and Technology, Laboratory for Mechanics of Materials and Nanostructures, Feuerwerkstrasse 39, 3602 Thun, Switzerland.

[d]EC2M, faculty of sciences 2, Campus Pierre Gemayel, Fanar, Lebanese University, 90656 Lebanon.

[1]Co-first authors

* Corresponding authors : mikhael.bechelany@umontpellier.fr, Phone: +33467149167, Fax: +33467149119

Ivo Utke: ivo.utke@empa.ch

ABSTRACT

We applied the core-shell concept to an urchin-inspired ZnO nanowire photoanode building block as a means to increase the electron transport and reduce recombination between nanowire and electrolyte. Dye-sensitized solar cells (DSSCs) were prepared, for the first time, from arrays of urchin-like ZnO nanowire building blocks covered with a thin layer of anatase TiO_2 by atomic layer deposition (ALD). An increase in the cell open-circuit voltage (V_{OC}) and

an improvement in the conversion efficiency were observed when the urchin-like ZnO building blocks were coated with 10 nm thick TiO_2 ALD shells in combination with 10 µm thick top layer of TiO_2 nanoparticles of 15.8 nm size. Using urchin-like ZnO nanowires as building blocks can improve the light-scattering and provide a higher surface area with a great control of the nanowire dimensions to increase the dye loading and reduce the electron collection path. The addition of a thin TiO_2 blocking layer decreases the recombination of charges in such a high surface area nanostructure.

GRAPHICAL ABSTRACT

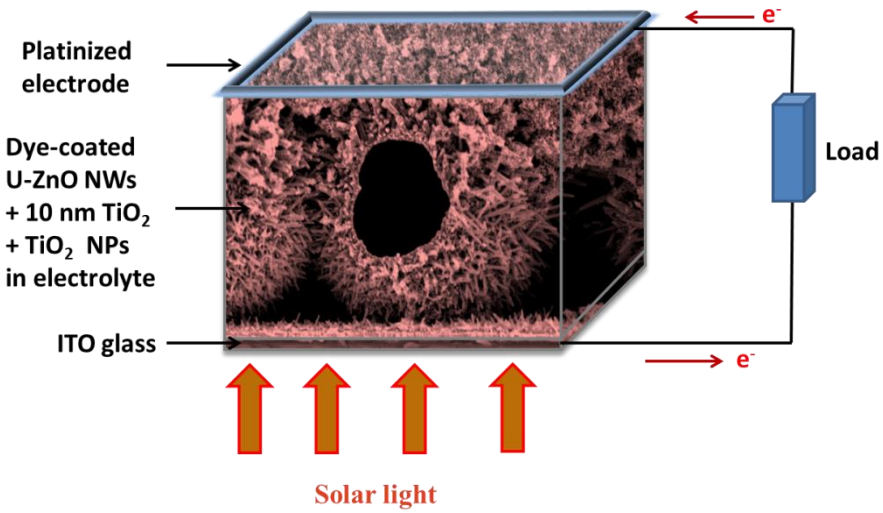

KEYWORDS

Dye sensitized solar cells, core-shell nanostructures, urchin-like ZnO nanowires, TiO_2, Atomic Layer Deposition

INTRODUCTION

The need to find an alternative to oil, and move towards clean and renewable energies, promotes since the last decades the emergence of new technologies. Among the different types of renewable energy, photovoltaic energy, based on the direct processing of the sunlight into electricity, has a significant potential [1]. One of the main objectives in this field of research is to reduce the processing costs of photovoltaic modules, using widely available and abundant materials which can be incorporated into a clean manufacturing processes, in order to create a genuine market competitor to other energy sources (fossil, nuclear, hydro), considered up to today as less costly. The dye-sensitized solar cell (DSSC) has become a promising alternative to commercial solar cells due to their low production cost and ease of fabrication [2-4]. In a DSSC, the photogenerated electrons at the light absorbing dye are injected to the conduction band of a wide band gap metal oxide nanostructure (*i.e.* TiO_2, ZnO), to be transported towards the current collector. Subsequently, the dye is regenerated by the redox couple of the electrolyte (*i.e.* I/I^{3-}) [5]. Conventional DSSCs consist of a mesoporous nanocrystalline TiO_2 film which possess a large surface area but with numerous grain boundaries, which ultimately increases the recombination rates of photogenerated electron-hole pairs and consequently lowers the photovoltaic efficiency [6, 7]. A major condition for electricity generation with a high photovoltaic efficiency is that the electron-hole pairs should not recombine (or very rarely). One goal of this study is suppressing the delicate balance between transport of charges and recombination of electron-hole pairs by using a specific architecture of semiconductor materials to accelerate electron transport and minimize recombination of electron-hole pairs by optimizing the nature, structure and dimensions of the semiconductors.

Alternatively, the use of semiconducting nanowires/nanotubes (e.g., ZnO, TiO_2, etc.) as the nanostructured photoanode offers several advantages such as a high surface area and a direct

electron transport owing to the lower amount of grain boundaries that both reduces the recombination of charges and increases the collection efficiency [8-10]. In addition, the unique geometry of the nanowires provides an improvement of the optical absorption and light trapping through a wide range of wavelengths, while reducing optical reflection [11].

Among the n-type semiconductor materials with large band gap, ZnO has been widely studied due to its non-toxicity and abundance on Earth [12]. For these reasons, ZnO nanowires are an ideal candidate for a nanostructured photoanode in DSSCs. While the direct electrical pathways to the electrode provided by the ZnO nanowires ensure the rapid collection of carriers generated throughout the device, it turns out that the conversion efficiency is limited by the surface area of the nanowire array [13-15]. These nanostructures have light harvesting efficiencies below 10 %, which can be improved by increasing the nanowire surface area with the control of the dimensions of each individual nanowire as reported in the literature [13, 15]. To tackle this challenge, we previously reported a novel approach to fabricate well-ordered arrays of hollow urchin-like single-crystal ZnO nanowire building blocks with controlled nanowire for photovoltaic applications [8, 16]. They were synthesized by combining the methods of auto-assembly of polystyrene spheres, atomic layer deposition (ALD), and electrodeposition (ECD) of ZnO nanowires. ALD and ECD are low-cost and large scalable process for the synthesis of hollow urchin-like ZnO nanowires. [17] This architecture combined the properties of 1D and 3D materials (higher surface area) and provided better control of the dimensions of the nanowires. The diameters, density and morphology of the nanomaterials were adjusted by tuning the growth parameters during the deposition (ALD and/or ECD), or by modifying the diameter of the PS. The opto-electronic, structural and morphological properties of these nanostructures impact the photovoltaic efficiency.

In this work, similar Urchin-inspired ZnO nanostructures were prepared and used as building blocks for the photoanode to fabricate DSSCs. The effect of the growth conditions on the conversion efficiency of the DSSCs was experimentally evaluated and discussed. Here we show that the recombination of charges in the urchin-inspired ZnO nanowires dye-sensitized cells could be decreased and the conversion efficiency enhanced by coating the urchin-like ZnO nanowire with a conformal TiO_2 shell deposited by ALD. ALD is a unique vapor-phase deposition technique of high quality conformal and homogenous thin films at relatively low temperatures with a precise thickness control. These properties are ideal for surface and interface engineering for next generation solar cells [18-21] . Many studies have described the effects of using insulating or semiconducting thin films of metal oxides as compact and blocking layers to reduce charge recombination at the different interfaces of the nanostructured solar cell. These films coating the transparent current collector (i.e. FTO) and/or the metal oxide nanostructure include Nb_2O_5, Al_2O_3, MgO, $SrTiO_3$, SiO_2, Y_2O_3, ZrO_2, SnO_2, and TiO_2 [22-27]. In general, a layer of oxide semiconductor plays an important role by passivating the surface defects of the metal oxide nanostructures, as well as adding an energy barrier that increases the separation between photoinjected electrons and the oxidized redox species in the electrolyte and consequently reduces recombination of charges [10]. These barrier recombination layers have to be thin enough to allow efficient photoelectron injection, and as the thickness decreases, the charge transfer resistance decreases. Therefore, this highlights the need of ALD to properly control the thickness of such layers. An overview of such layers deposited using different techniques can be found in reference [28]. A lower rate of recombination can be translated as a lower dark current (J_{dark}) and a higher open-circuit voltage (and fill factor) of a DSSC according to the general expression of the cell open-circuit voltage (V_{OC}): $V_{OC} = nV_{th} \ln((J_{SC}/J_{dark}) + 1)$, where n is the diode ideality factor and V_{th} is the thermal voltage [29]. In addition to reduce the recombination, an energy barrier shell can

pointedly increase cell V_{OC} directly if it creates a dipole at the core-shell interface that shifts the band edge of the core upward in energy [25].

Until now, low conversion efficiencies were obtained when using ZnO nanowires [30], ZnO nanotubes [31] or ZnO nanoparticles [3, 32] as building blocks for DSSCs. We describe, for the first time, the ability of a 3D architecture based on urchin-like ZnO nanowires with larger surface area coated with TiO_2 nanostructure to enhance the performance of the DSSCs. Applying the core-shell concept to an urchin-inspired single crystal ZnO nanowire photoanode building block as demonstrated in this work provides a means to increase the electron transport and reduce recombination between nanowire and electrolyte.

MATERIALS AND METHODS

1. Deposition of polystyrene microsphere

A commercially available suspension of polystyrene microsphere (PS) (diameter ~ 5 µm, 4 wt% aqueous dispersion) from Thermo fisher, USA, was used for dip coating transparent Indium doped tin oxide (ITO) deposited on glass (size 1 x 5 cm^2) purchased from Kintec Company, Hong Kong. Before making the deposition of spheres on the ITO glass, the substrate was subjected to a specific cleaning technique to remove surface dirt (grease, dust etc.) collected after manufacturing and during the storage. The cleaning method included, first, washing the substrates with commercial soap and hot water (~ 90 °C) followed by rinsing with ultra-purified water. Then the substrates were soaked for 15 minutes in an ultrasonic bath at 70 °C in three different solvents: trichloroethylene, acetone and isopropanol and in between rinsed with ultra-pure water heated to 90 °C. The resulting substrates were dried and stored in plastic boxes to prevent possible contamination prior to deposition. 200 µL of a carboxylate modified PS microsphere suspension was diluted in 150 µL of ethanol and

then dispersed (drop-by-drop using a micro-pipette) onto the surface of deionized water filled into a Petri dish of 5 cm in diameter to self-assemble for about 12 hours. An ITO substrate was exposed under a UV lamp for 10 min to promote the adherence of the PS spheres on the surface of the substrate and then immersed into the suspension. The polystyrene sphere monolayer was transferred onto the ITO substrate surface by slow removal from the solution at an angle of 45° [16]. After complete drying of the PS-covered ITO/glass substrate in furnace at 100 °C for 30 min, the regularly arranged and closely packed spheres were reduced in diameter using an oxygen plasma treatment by fixing the pressure at 0.7 mbar and the power supply at 0.2 A. The size of the polystyrene spheres was very accurately controlled by choosing the appropriate plasma exposure time [6].

2. Synthesis of ZnO Urchins

The ITO covered with PS (ITO/PS) was introduced into a custom made atomic layer deposition (ALD) reactor for deposition of a ZnO thin film covering homogeneously the spheres and the ITO substrate surface [9]. The ZnO_{ALD} thin films play two important roles: it is used as a seed layer that controls the growth of the ZnO nanowires, and it renders the surface electrically active to be used as a conductive electrode for electrodeposition. The ZnO_{ALD} thin films were deposited using diethylzinc (DEZ) and water (H_2O). Diethyl Zinc (DEZ) ($Zn(CH_2CH_3)_2$, 95% purity, CAS: 557-20-0) was purchased from Sigma Aldrich and used as zinc source. The ALD was performed by sequential exposures of DEZ and H_2O separated by Argon purge at a flow rate of 100 standard cubic centimeters per minute (sccm). The regime for the deposition of ZnO consisted of 0.2 s pulses of DEZ, 40 s of exposure to DEZ, 60 s of Argon purge followed by 2 s pulse of H_2O, 40 s exposure to H_2O, and a final 60 s Argon purge [16]. This constituted one cycle. ZnO films with 100 ALD cycles were

deposited on ITO glass substrates for obtaining 20 nm thick layers of ZnO. The temperature was fixed at 80°C. The ITO/PS/ZnO_{ALD} ensemble was then used as a working electrode for the electrodeposition of ZnO nanowires by bubbling the oxygen in a three-electrode electrochemical cell. A platinum wire was used as the counter electrode and an Ag/AgCl electrode as the reference electrode. The electrolyte was an aqueous solution saturated by molecular O_2 containing zinc chloride as zinc precursor (5.10^{-4} M) and potassium chloride (0.1M) as salt. The electrodeposition was performed for a period of 2 to 4 hours by fixing the potential (-1 V) versus the reference electrode) using an Autolab VERSASTAT3 potentiostat. The bath temperature was set to 80°C. After electrodeposition, the samples were annealed in air at 450 °C for 1h to ensure the removal of the PS spheres and the enhancement of the ZnO nanowires crystallinity. The above process steps defined the hollow urchin-like ZnO nanowires (U-ZnO NWs) building blocks.

3. Atomic Layer Deposition of TiO_2 and Dye-sensitized solar cell Fabrication

The core-shell concept was realized by transferring the urchin-like ZnO nanowires into a built-in ALD reactor to deposit conformal thin films of TiO_2 as recombination barrier layers with different thicknesses (5, 10, 15, 20, 34 and 42 nm). The deposition of TiO_2 was performed onto the urchin-like ZnO nanowires at a reactor temperature of 60 °C by alternating the precursors of Titanium Tetra-Isopropoxide (TTIP) heated to 90 °C and H_2O heated to 40 °C. One ALD cycle consisted of a TTIP pulse of 5 s followed by a 10 s exposure, and 60 s purge, followed by a H_2O pulse of 2 s with 10 s exposure and 60 s purge. For some of the samples, a mesoporous film of TiO_2 anatase nanoparticles (P25 Solaronix) was deposited by doctor blade technique on top of the ZnO/TiO_2 core-shell structures.

The samples were then heated to 450 °C in air for 30 min and then immersed in a solution of 12 mg of Ru dye (N719, Solaronix) diluted in 30 mL of methanol for 12 h. In

order to fabricate the cell, the films were rinsed with ethanol, dried, and sandwiched together to a platinum counter electrode separated by a 60-μm-thick hot-melt film (Solaronix). The internal space of each cell was filled with an iodide electrolyte (AN-50, Solaronix). Cells were immediately tested under simulated sunlight and illuminated through a black cover with an aperture of 0.6 cm^2.

4. Characterization

The morphology of the samples was observed by scanning electron microscopy (SEM, Hitachi S-4800). In order to know the elemental composition of samples, energy dispersive X-ray spectroscopy (EDX) was performed on a JEOL JEM 2200 fs microscope, operated at 200 kV. X-ray diffraction data were obtained on a Bruker D-8 GADDS diffractometer (Co Kα) to determine the crystalline structures and orientation. Raman spectra were obtained on a Raman microscope (Nova Spectra, ND-MDT) featuring a laser source with a wavelength of 532 nm and a 50× objective lens with a numerical aperture of 0.75. Spectra were recorded at a spectral resolution of 2.7 cm^{-1} with a laser power below 100 μW so that it does not induce phase transformation of TiO_2; the exposure time was 30 s for all the samples.

The reflectivity of the TiO_2-hollow U-ZnO NW building blocks and the absorbance of TiO_2 core-shell U-ZnO NW building blocks were characterized by a spectrophotometer from Perkin Elmer (Lambda 900). The illumination was carried out from the glass/ ITO side. Current–voltage (J–V) measurements were made on the DSSCs under half sun illumination (500 $W.m^{-2}$). The characteristic parameters of the solar cells, including short-circuit current density (J_{sc}), open-circuit voltage (V_{oc}), fill factor (FF) and overall photoconversion efficiency were extracted from the J–V curves.

RESULTS AND DISCUSSION

1. Synthesis and characterization of U-ZnO NWs

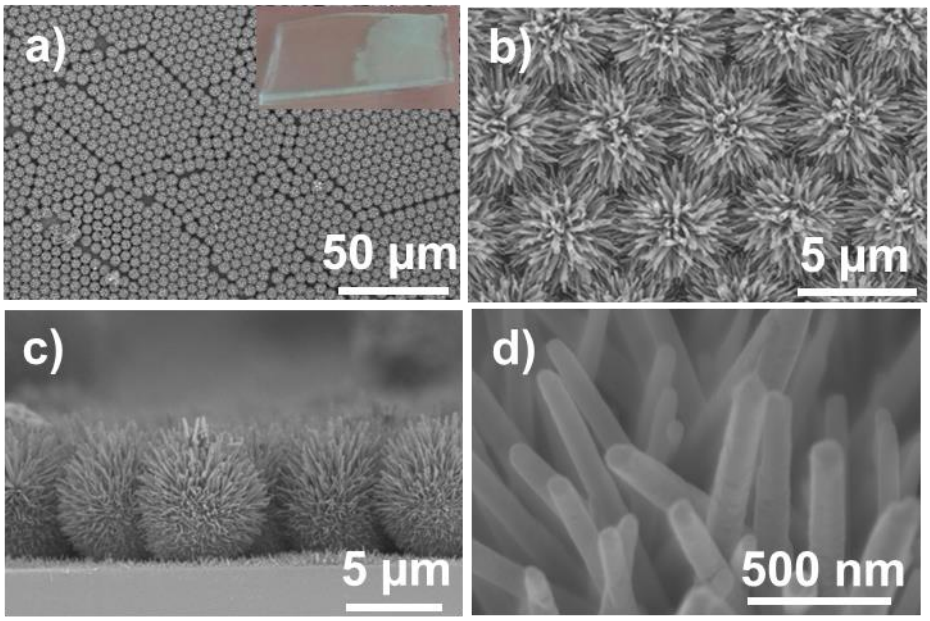

Figure 1. SEM images of the U-ZnO NWs: (a) regularly arranged urchin-like ZnO nanowires. The inset shows a macroscopic view of the deposition. (b) Higher resolution of U-ZnO NWs after 25 min of PS plasma etching treatment. (c) longitudinal cross sections showing the growth of ZnO nanowires on the PS and in the gap between them. (d) views of individual U-ZnO NWs grown on the 20 nm thick ALD ZnO coated PS spheres after plasma etching treatment of 25 min.

To obtain the unique architecture of U-ZnO NWs, several steps were used, such as: (i) deposition of an ordered monolayer of PS spheres by dip coating onto an indium doped tin oxide (ITO) glass substrate, (ii) reduction of the size of the spheres by plasma etching treatment, (iii) deposition of a uniform conformal thin layer of ZnO (~ 20 nm) by atomic layer deposition (100 cycles) which renders the surface covered by PS spheres electrically active for subsequent electrodeposition. In addition, this thin ALD ZnO seed layer serves as a compact recombination barrier layer to prevent backflow of electrons and avoid short-circuits between the ITO glass electrode and the electrolyte [33], (iv) electrodeposition of the ZnO

nanowires onto the ITO/PS/ZnO_{ALD} [34, 35], and (v) removal of polystyrene spheres by annealing at 450 °C for 1h.

The resulting organized arrays of U-ZnO NWs are deposited on the entire surface of the samples as presented by SEM image in Figure 1a. The inset is a macroscopic view of the sample which shows the uniformity of the deposition. By increasing the time of the plasma etching treatment, it is possible to control the spacing and the overall size of the urchin structures. The etching of PS spheres monolayers was performed with 25 min or with 30 min of plasma (Figure S1a and b). After 25 min of treatment, the size of the spheres decreased from 5 µm to 4 µm leaving 1 µm spacing between the spheres whereas after longer treatment time (30 min), the size of the spheres decreased from 5 µm to 3.5 µm leaving 1.5 µm spacing between the spheres (Figure S1a and b). The SEM images (Figure 1a - d) present the resulting ordered urchin-like structures obtained after 25 min of treatment. The time of etching was optimized in order to have a large fraction of the U-ZnO NWs surface exposed to the incident light. The ZnO NWs are characterized by 948 nm long (Figure 1c) and a diameter of 57 nm (Figure 1d) when the thickness of the ZnO ALD layer is 20 nm. The density of the ZnO nanowires is 5260 NWs/urchin. The overall active surface area of the urchin-like ZnO NWs is 42.25 cm^2 compared to 17.8 cm^2 for the ZnO NWs on a flat substrate (Figure S6 in the Supporting Information). The growth of the nanowires between the urchin nanostructures was also observed (Figure 1c), which also participates to increase the overall surface area.

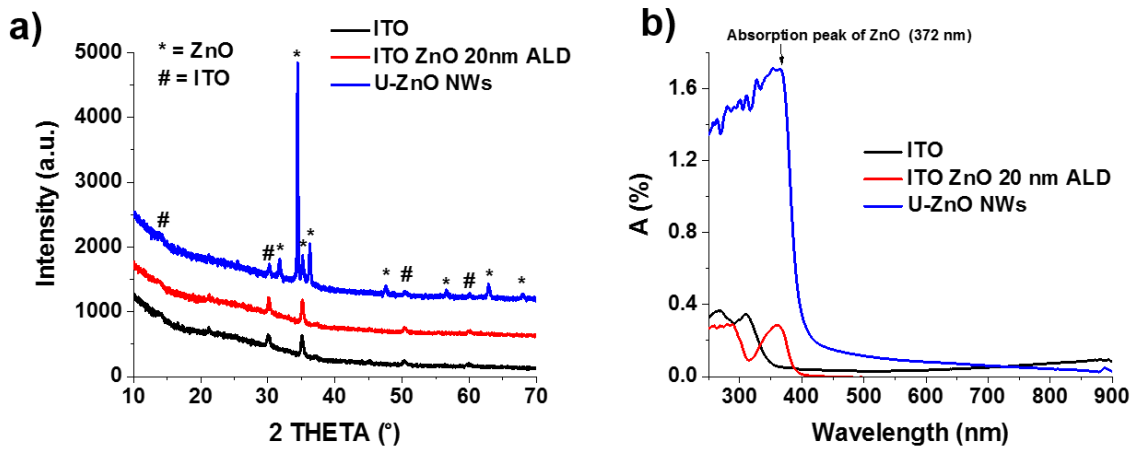

Figure 2. a) X-ray diffractograms and **b)** Absorption spectra of ZnO 20 nm ALD layer on a flat ITO glass substrate and U-ZnO NWs.

EDX analysis confirmed the presence of ZnO as indicated in Table S1. The X-ray diffraction spectrum of the U-ZnO NWs presented in Figure 2a shows the characteristic peaks of the ZnO wurtzite structure. The main orientations of the ZnO NWs are (100) at 34.4°, (002) at 35.2°, and (101) at 36.3° (Figure 2a).

In order to study the influence of U-ZnO NWs on the light scattering, the spectral dependence of the absorption of the samples was measured (Figure 2b). For all analyzed samples based on ZnO, the spectra show UV absorbance edge close to 375 nm (3.3 eV), which corresponds to the band gap energy of ZnO. No absorbance was shown for bare ITO glass sample. The presence of higher absorbance values is due to the presence of higher quantity of ZnO. Especially, the formation of urchins increases significantly the absorption by 30% at 372 nm which supports the stronger advantage of using the high surface area U-ZnO NWs to enhance the light scattering.

2. U-ZnO-TiO_2 core-shell nanostructures

2. 1. Synthesis of U-ZnO-TiO_2

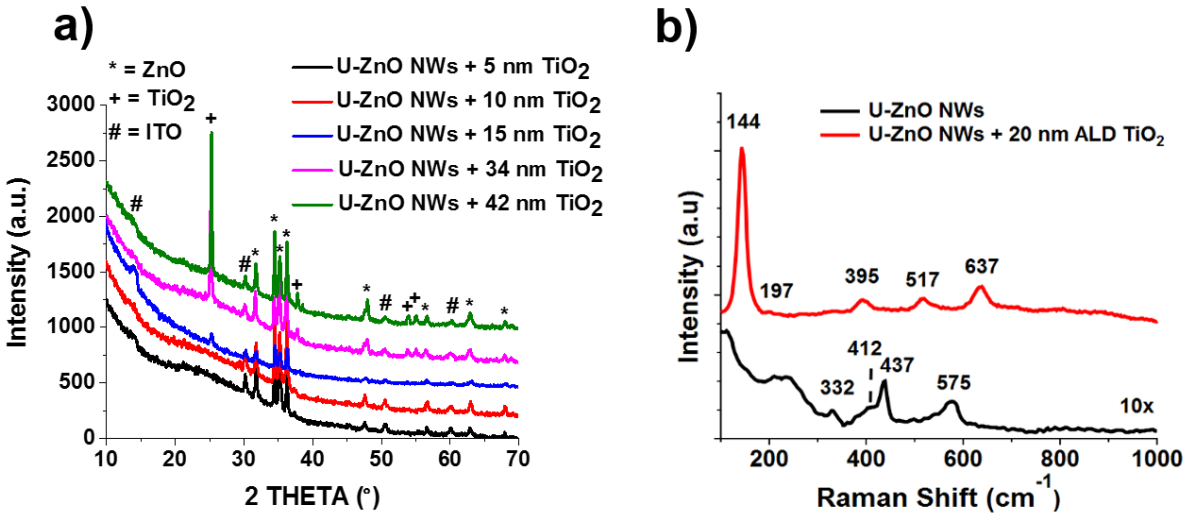

Figure 3. a) X-ray diffraction pattern of U-ZnO NWs on ITO glass substrates covered with different thicknesses of TiO_2 layer and **b)** Raman spectra of U-ZnO NWs and U-ZnO NWs/ TiO_2 shell.

A uniform conformal and amorphous thin layer of TiO_2 with different thicknesses (5 nm, 10 nm, 15 nm, 20 nm, 34 nm, 42 nm) was deposited by ALD at 60 °C with a growth rate of 0.056 nm/cycle (measured on Si substrates).The samples were then annealed at 450 °C in air for 30 min in order to obtain the anatase phase. The X-ray diffraction (Figure 3a) points out a peak at 25° characteristic of the anatase phase (101) of TiO_2 for the samples based on U-ZnO NWs covered with different thicknesses of TiO_2 ALD layer. Reasonably, the anatase peak becomes more intense when the thickness of the TiO_2 layer increases. The average grain size, calculated from the (101) peak of anatase TiO_2 using the Scherrer formula, was 33.0 nm, 50.5 nm and 65.7 nm for the U-ZnO NWs/ TiO_2 ensemble with a thickness of TiO_2 layer of 15 nm, 34 nm and 42 nm, respectively. The X-ray diffraction spectrum shows also the peaks characteristic of ZnO wurtzite and ITO deposited on the glass substrates (Figure 3a). The anatase phase of TiO_2 was also evidenced by Raman showing the characteristic peaks at 144 cm^{-1}, 197 cm^{-1}, 396 cm^{-1}, 517 cm^{-1} and 637 cm^{-1} (Figure 3b) for the sample based on U-ZnO

NWs / $TiO_{2\ 20\ nm\ layer}$ ensemble. In the case of the reference sample based on U-ZnO NWs without TiO_2, only peaks of ZnO were observed.

2. 2. Characterization of U-ZnO-TiO_2

The spectral dependence of the transmittance of the samples was studied before (Fig. S3a in the Supporting Information) and after dye loading and subsequent illumination (Fig. S3b), in order to determine the effect of the thickness of the TiO_2 shell on light scattering and dye loading. A small decrease of the transmittance from 70% to 55% was observed for the sample U-ZnO NWs/ $TiO_{2\ layer}$ when increasing the thickness of the TiO_2 layer (Figure S3a). The reference sample based on U-ZnO NWs without TiO_2 has the highest transmittance. The decrease of the transmittance can be explained by the fact that the thick layer of TiO_2 (from 20 nm to 42 nm) absorbs photons and reduces light scattering to the ZnO. This hypothesis will be analyzed later with the study of the J-V curves of the samples.

The spectral dependence of the transmittance of the samples was also measured after dye loading and illumination, as shown in Figure S3b. An increase of absorption in the wavelength range of the excitation of the TiO_2 is noticed when increasing the thickness of $TiO_{2\ layer}$ (34 nm and 42 nm) as a consequence of the higher amount of dye loading (Figure S3b) [36].

The spectral dependence of the optical reflectance of the samples based on U-ZnO NWs with various thickness of TiO_2 shell was also studied (Figure S4 in the Supporting Information). By increasing the thickness of the TiO_2 layer deposited on the U-ZnO NWs, the maximum of the total reflectance (at λ= 430 nm) increases from 20% to 35% for 5 to 20 nm TiO_2 thickness, respectively, along with a decrease of the reflectance over the whole wavelength range (Figure S4).

2. 3. Solar cell performance of core-shell U-ZnO-TiO_2

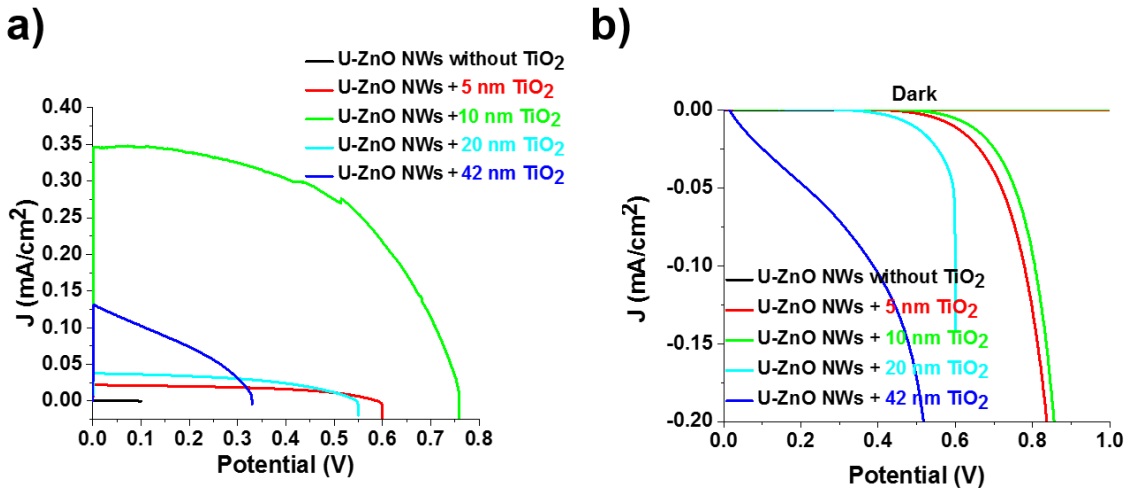

Figure 4. *J-V* data for DSSC samples based on U-ZnO NWs-TiO_2 core-shell cells with different thicknesses of TiO_2 shell. Each cell was sensitized in dye solution for 12 h. **(a)** Power plots under **500 Wm^{-2}** simulated sunlight of U-ZnO NWs coated with TiO_2 of different thicknesses and **(b)** dark.

The effect of the thickness of TiO_2 on the light scattering has been discussed. The photovoltaic efficiencies were studied by analyzing the J-V curves obtained for the DSSC samples based on ZnO/ TiO_2 core-shell with various TiO_2 shell (Figure 4). Current–voltage (J-V) measurements on the DSSCs were performed under full sun illumination, half sun illumination (500 Wm^{-2}) and dark. The characteristic parameters of the solar cells, including short-circuit current density (J_{sc}), open-circuit voltage (V_{oc}), fill factor (FF) and overall photoconversion efficiency (µ (%)) were extracted from the J-V curves.

Figure 4a presents the *J-V* curves for the samples of U-ZnO NWs/ TiO_2 core shell under 500 Wm^{-2} coated with different thicknesses of TiO_2 and sensitized in Ru dye for 12 h. The plots also include uncoated U-ZnO NWs cells sensitized in Ru dye for 12 h as a reference cell. The addition of a 10 nm layer of TiO_2 to the U-ZnO NWs cells results in a working cell with an overall efficiency increase from 0 to 0.28%, (the fill factor (FF) jumps from 0.04 to

0.55 (a 90% improvement), and the J_{SC} jumps from 0 to 0.34 (Figure 4a and table 1). Thus, an improvement in cell efficiency was observed after adding a 10 nm layer of TiO_2 (Figure 4a). For TiO_2 shells thicker than 10 nm (20 nm-42 nm), the V_{OC} decreases by about 430 mV from 0.76 V to 0.33 V and the FF decreases from 0.55 to 0.34. For J_{SC}, the current falls from 0.34 to 0.13 (table 1). The plots in Figure 4b show the dark current J_{dark} of the DSSC cells. The improvement of the Voc for the thinner TiO_2 coatings suggests a reduction in charge recombination compared to the thicker coatings. Thicker coatings lead to slower charge transport and shorter electron lifetimes resulting in more recombination of charges, evidence by the higher dark currents. This has been reported to be caused by the positive shift of the conduction band of TiO_2 as the thickness increases [36].

Thus, the thickness of TiO_2 layer has a significant influence on the cell efficiency of the device. The TiO_2 blocking layer has to be sufficiently thin to allow electron injection to the ZnO, but with a high surface coverage of the nanostructure and thick enough to prevent the back reaction of electrons. The cell efficiency has almost tripled by only increasing the thickness of TiO_2 layer from 5 nm to 10 nm while the V_{OC} and FF increase slightly from 0.6 V to 0.76 V and from 0.5 to 0.55, respectively (Figure 4a and table 1).

Table 1. Dependence of V_{OC}, FF, J_{dark}, J_{SC}, and efficiency with the thickness of TiO_2 layer.

Samples (U-ZnO NWs/ TiO_2 ALD layer)	**V_{OC}** (V)	**FF** (mV)	**J_{SC}** (mA cm^{-2})	**Efficiency** (%)
0 nm TiO_2	0.10	0.04	0	**0**
5 nm TiO_2	0.60	0.50	0.02	**0.01**
10 nm TiO_2	0.76	0.55	0.34	**0.28**

20 nm TiO_2	0.55	0.47	0.04	**0.02**
42 nm TiO_2	0.33	0.34	0.13	**0.03**

3. Hybrid structure of nanoparticles and urchins

3.1. Synthesis and characterization of TiO_2 nanoparticle on core-shell U-ZnO-TiO_2

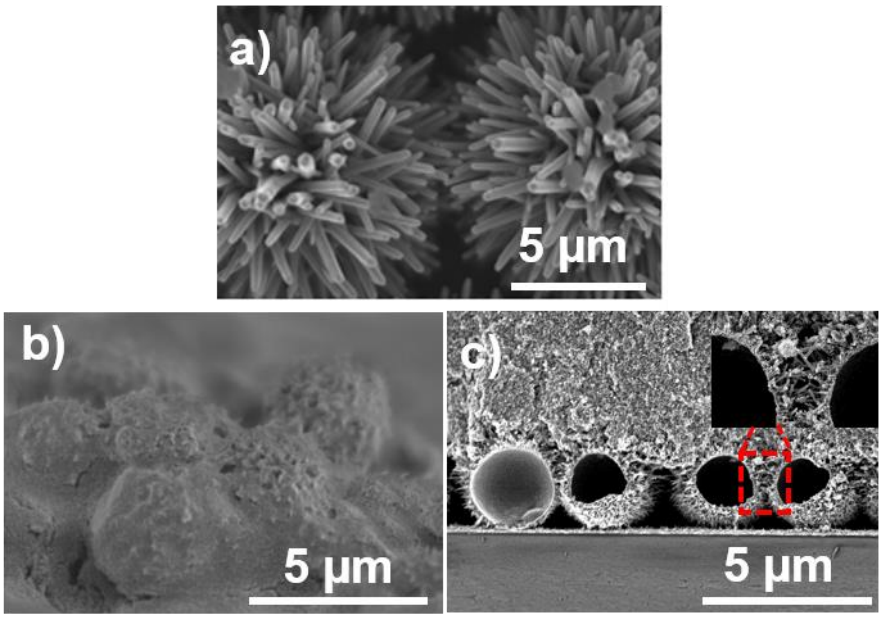

Figure 5. SEM images of urchin-inspired ZnO-TiO_2 core-shell and TiO_2 nanoparticle cells. (a) growth of U-ZnO $_{NWs}$ on 20 nm of ZnO_{ALD} seed layer deposited on PS spheres treated with 25 min of PE treatment; The urchins based ZnO NWs were covered with 10 nm TiO_2 anatase (b) U-ZnO $_{NWs}$ / $TiO_{2\ 10\ nm\ layer}$ / $TiO_{2\ NPs}$ ensemble; and (c) inset shows the presence of $TiO_{2\ NPs}$ on the ZnO NWs.

A mesoporous film (10 µm) of anatase TiO_2 nanoparticles ($TiO_{2\ NPs}$) was deposited on the ZnO / $TiO_{2\ 10\ nm\ layer}$ ensemble in order to further increase the surface area (Fig. 5b and c). The commercial TiO_2 nanoparticles provide a surface area of ~ 100 m^2/g (after firing) and a pore size of 15-20 nm. The overall surface area obtained for the urchins-based ZnO NWs coated with TiO_2 NPs is ~ 113.76 m^2/g. Figure 5a presents the urchins based ZnO NWs

covered with 10 nm TiO_2 anatase without the presence of $TiO_{2\ NPs}$. Figure 5c shows that the mesoporous TiO_2 film does not infiltrate in between the urchins but rather is supported by them.

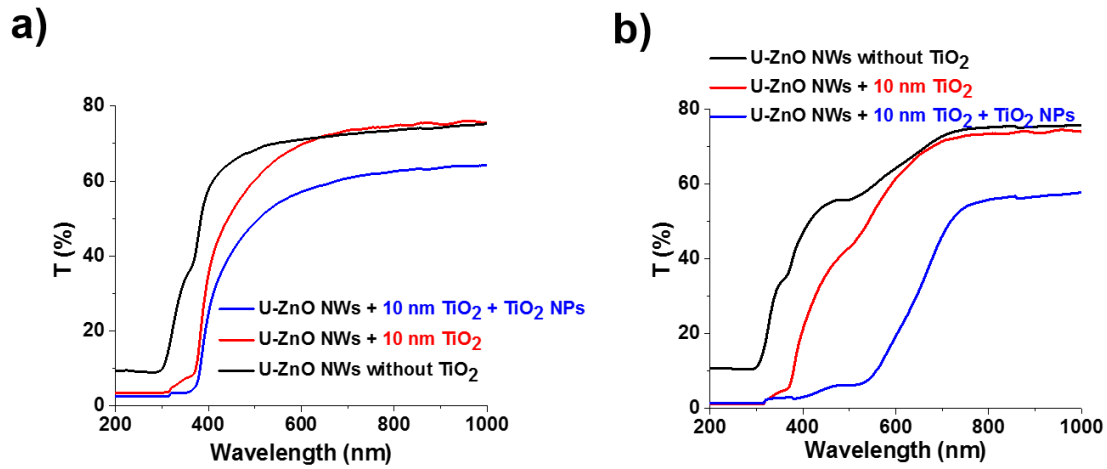

Figure 6. Transmittance spectra of the DSSC based on U-ZnO $_{NWs}$ / $TiO_{2\ 10\ nm\ layer}$ core-shell and U-ZnO $_{NWs}$ / $TiO_{2\ 10\ nm\ layer}$ / $TiO_{2\ NPs}$ cells (a) before and (b) after illumination.

The influence of the mesoporous film (10 µm) of TiO_2 nanoparticles ($TiO_{2\ NPs}$) on the ZnO / $TiO_{2\ 10\ nm\ layer}$ ensemble was studied to determine the spectral dependence of the transmittance of the samples before (Figure 6a) and after illumination (Figure 6b).

For U-ZnO NWs/ $TiO_{2\ 10\ nm\ layer}$/ $TiO_{2\ NPs}$, the transmittance decreases from 75% to 60% after adding TiO_2 nanoparticles as compared with U-ZnO NWs/ $TiO_{2\ 10\ nm\ layer}$ without TiO_2 nanoparticles, owing to the presence of a thick mesoporous layer of TiO_2 nanoparticles with larger surface area and consequently a larger amount of dye adsorbed as shown in Figure 6b. The reference sample based on U-ZnO NWs without TiO_2 has the highest transmittance. Furthermore, adding TiO_2 nanoparticles on the U-ZnO NWs covered with 10 nm layer of TiO_2 can enhance even more the surface area and dye loading and consequently increase the conversion efficiency of the DSSC.

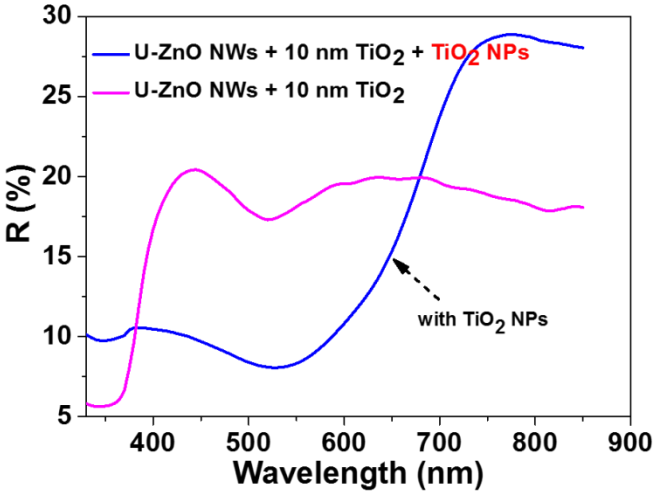

Figure 7. Reflectance spectra of the DSSC based on U-ZnO NWs/ $TiO_{2\ 10\ nm\ layer}$ core-shell after illumination as a function of the addition of TiO_2 NPs.

The spectral dependence of the optical reflectance of the U-ZnO $_{NWs}$ / $TiO_{2\ 10\ nm\ layer}$ core-shell and U-ZnO $_{NWs}$ / $TiO_{2\ 10\ nm\ layer}$ / $TiO_{2\ NPs}$ cells was also studied (Figure 7). In our three-dimensional architecture based on U-ZnO NWs, the increase of the reflectivity covers a large wavelength range (400-800 nm). This can be explained due to the fact that nanowires from ZnO urchins are exposed to the incident light from all angles thanks to the 3D-architecture. As shown and explained in the transmittance spectra of the DSSC based on ZnO/ TiO_2 core-shell after illumination, a broadening in the wavelength range of the reflectance was noticed after adding TiO_2 nanoparticles to the DSSC based on U-ZnO NWs/ TiO_2 layer due to the thick layer of TiO_2 nanoparticles (10 µm). The total reflectance (at λ= 600 nm) increased from 16% to 28% for 10 µm thickness of TiO_2 nanoparticles.

3.2. Solar cell performance of hybrid nanoparticle core shell structure

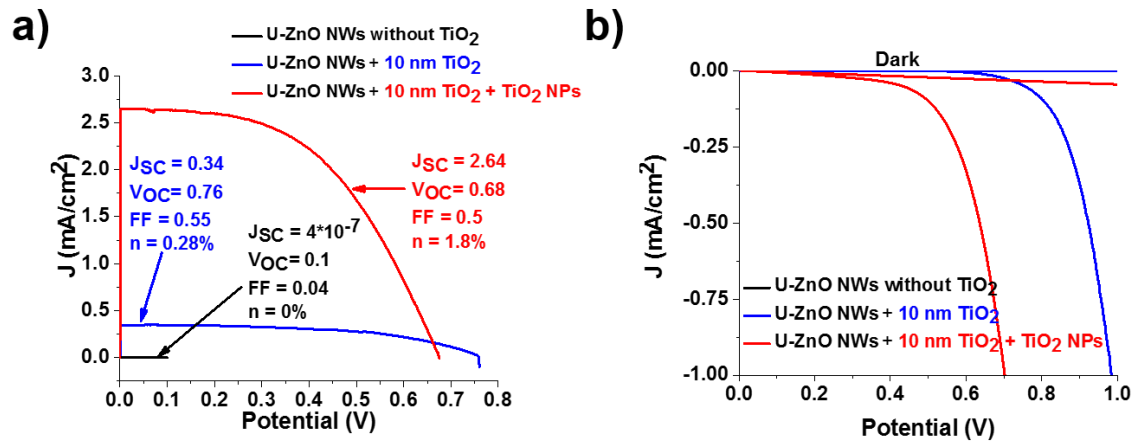

Figure 8. *J-V* data for DSSC samples based on U-ZnO NWs/ TiO_2 (10 nm layer) core-shell cells with and without the addition of TiO_2 nanoparticles. Each cell was sensitized in dye solution for 12 h. Power plots **(a)** under **500 Wm^{-2}** simulated sunlight and **(b)** dark**.** The short-circuit current density (J_{sc}), the open-circuit voltage (V_{oc}), the fill factor (FF) and the overall photoconversion efficiency (μ (%)) are specified for each device.

A considerable improvement of the characteristic parameters of the solar cell based on U-ZnO NWs/ TiO_2 (10 nm layer) was observed after adding TiO_2 nanoparticles (U-ZnO NWs/ TiO_2 (10 nm layer)/ TiO_2 NPs): the cell efficiency improved from 0.28% to 1.8% and the J_{SC} increased from 0.34% to 2.64%. The V_{OC} decreases slightly from 0.76 V to 0.68 V, while the FF remains almost the same value (0.5) (Figure 8a and table 2). The improvement in cell efficiency using the U-ZnO NWs/ TiO_2 (10 nm layer) in combination with the TiO_2 nanoparticles is mainly due to the increase in surface area and thus the dye loading. However, low electron transport and recombination mechanisms due to the grain boundaries and surface defects are still present in the mesoporous TiO_2 NP film, as observed from the high dark currents (Figure 8b). This effect can be further improved by depositing a thin blocking layer onto the NPs, as reported elsewhere[37]. It has to be noted that the photogenerated electrons from the adsorbed dye at the mesoporous TiO_2 layer are transported through the TiO_2 coated

U-ZnO NWs, this film is only in contact with the urchins and not the substrate as observed from Figure 5c.

We also fabricated a DSSC based only on a 10 µm mesoporous film of TiO_2 NPs using the same fabrication method as for the U-ZnO NWs/ TiO_2 (10 nm layer)/ TiO_2 NPs as a benchmark to compare to the cells based on a hybrid structure of urchins and TiO_2 nanoparticles. The overall efficiency of such DSSC was found to be 1.5% (see Table 2). This is rather low compared to what is reported in literature, but nevertheless it serves as a comparison to show the potential of the U-ZnO NWs as conductive nanoscaffold.

Thereby, the highest characteristic parameters were obtained for the DSSC based on U-ZnO NWs/ TiO_2 (10 nm layer)/ TiO_2 NPs (J_{SC} = 2.64 mA/cm^2, V_{OC} = 0.68 V, FF= 0.5, µ = 1.8%, J_{dark} = 4.6 mA/cm^2).

Table 2. Dependence of V_{OC}, FF, J_{dark}, J_{SC}, and efficiency with the thickness of TiO_2 layer in the presence of TiO_2 NPs.

Samples (U-ZnO NWs/ TiO_2 ALD layer)	**V_{OC} (V)**	**FF (mV)**	**J_{SC} (mA cm^{-2})**	**Efficiency (%)**
5 nm TiO_2	0.6	0.5	0.02	**0.01**
5 nm TiO_2 + TiO_2 NPs (10 µm**)**	0.61	0.49	1.03	**0.62**
10 nm TiO_2	0.76	0.55	0.34	**0.28**
10 nm TiO_2 + TiO_2 NPs (10 µm**)**	0.68	0.5	2.64	**1.8**
TiO_2 NPs (10 µm**)**	0.64	0.59	2.03	**1.5**

4. Discussion

Table 1 summarizes the V_{OC}, FF, J_{SC}, and efficiency as a function of the thickness of the TiO_2 layer. The V_{OC} and FF increase to 0.76 V and 0.55, respectively, after the deposition of a 10 nm layer of TiO_2, which then gradually decrease by increasing the thickness of the TiO_2 layer (20 nm and 42 nm). Increasing the thickness of the TiO_2 layer reduces the light scattering to the ZnO and decreases the electron injection to the ZnO, whereas the thin TiO_2 coatings reduce the recombination of charges at the interface while still allowing electron injection to the ZnO, as observed from the low dark currents.

After adding TiO_2 nanoparticles to the U-ZnO NWs – 10 nm TiO_2 layer ensemble, the surface area increases and consequently the dye loading, therefore the overall efficiency increases up to 1.8 %, regardless of the slight decrease in the V_{OC} (from 0.76 to 0.68 V) (Table 2). The TiO_2 nanoparticles are still subjected to recombination mechanisms and thus the significant reduction of the V_{oc} onset from dark measurements (Figure 8b). These data clearly show that thin TiO_2 shells enhance V_{OC} and fill factor by reducing the recombination of electron hole pairs at the oxide-electrolyte interface, which strongly depend on the thickness of this TiO_2 layer (Table 1), highlighting once more the need of ALD to precisely control the thickness of the film.

Hence, these results show an improvement of the conversion efficiency to 1.8% compared to 0.8% and 0.7% for ZnO nanowires [14, 30, 38], 0.6% for ZnO nanoparticles [3, 32] and even lower efficiency (0.29%) [31] for ZnO nanotubes through the specific geometry of ZnO urchins nanowire arrays, and 1.3% for urchins inspired ZnO nanowires [8] by including a TiO_2 recombination barrier layer. The ALD TiO_2 layer reduces the recombination rate of photo injected electrons in the U-ZnO structure that otherwise would have recombined with either a surface defect or the electrolyte in contact with the U-ZnO structure. The

combination of the coated U-ZnO with a mesoporous film of TiO_2 nanoparticles increased the amount of adsorbed dye, increasing the photocurrent and therefore improved the characteristic parameters of the solar cell. Although, our actual cell efficiencies are still lower than standard nanoparticle-based solar cells, we demonstrated the use of U-ZnO coated with ALD TiO_2 as a conductive scaffold, as the majority of the current was transported through the urchins. We believe that there is a possibility to further improve the conversion efficiency by further optimization of the total surface area of the U-ZnO NWs in addition to the mesoporous TiO_2 film or by using a film of perovskite absorber as the light-harvesting active layer [39, 40].

CONCLUSION

Core-shell DSSC cells were fabricated and characterized. The unique 3D architecture of urchin-like ZnO nanowire arrays have increased the absorbed amount of light due to its larger surface area compared to ZnO nanowires. The urchin-like ZnO nanowires were prepared by a low cost technique electrodeposition of ZnO nanowires on polystyrene spheres coated with 20 nm of ZnO by ALD. The resulting U-ZnO nanostructures were coated with conformal and amorphous TiO_2 shells by ALD which were annealed at 450 °C in order to obtain the anatase phase. These nanostructures were then sensitized with a solution of Ru dye (N719). Coating the U-ZnO NWs with 5-10 nm of anatase TiO_2 has reduced the recombination of charges, improved the J_{SC}, V_{OC}, FF and consequently the overall conversion efficiency. For TiO_2 shells thicker than 10 nm (20 nm - 42 nm), the transmittance decreases due to a larger absorption of photons from TiO_2, reducing light scattering to the ZnO. Even though thicker TiO_2 layers can adsorb more dye, they lead to lower charge transport resulting in more recombination of charges, as observed from the higher dark currents. A considerable improvement of the characteristic parameters of the solar cell was observed after adding a mesoporous film of TiO_2 nanoparticles. Adding TiO_2 nanoparticles on the TiO_2 coated U-ZnO NWs can increase

further the surface area and consequently increase the conversion efficiency of the DSSC, most likely due to the larger dye loading. Nevertheless, the large surface area of the nanoparticles, grain boundaries and surface defects still lead to recombination of charges, which limits the full potential of the cell, which can be improved by depositing another thin blocking layer to the NPs. Ultimately, it is worth mentioning that the photogenerated current was transported in its majority through the U-ZnO, which evidences the high conductivity of such nanostructures, and further optimization may improve the overall conversion efficiency.

ACKNOWLEDGMENTS

This work was financially supported by the joint funding program from the Lebanese National Council for Scientific Research CNRS-L and the University of Montpellier UM. Dr. N. Abboud, would like to thank the National Council for Scientific Research in Lebanon for the support in funding this work. This work was partially supported by CNRS project (PICS 2015-2017 number 233977 NANOALD).

AUTHORS' CONTRIBUTION

Chantal Karam, Ziad Herro, Nadine Abboud, Sophie Tingry did the electrodeposition and characterizations of Urchin-Inspired ZnO Nanowires; Mikhael Bechelany and Philippe Miele did experiments on Atomic layer deposition of ZnO and analyzed the results; Chantal Karam, Carlos Guerra-Nuñez, Roland Habchi, Antonio Khoury, did the physico-chemical characterization of the obtained materials and analyzed the obtained results; Chantal Karam, Ivo Utke and Carlos Guerra-Nuñez did experiments on Atomic layer deposition of TiO_2 and Dye Sensitized Solar Cells; Ivo Utke and Mikhael Bechelany designed the works and write the manuscript.

REFERENCES

1. Makrides, G.Z., Bastian Norton, Matthew Georghiou, George E. Schubert, Markus Werner, Jürgen H., *Potential of photovoltaic systems in countries with high solar irradiation.* Renewable and Sustainable Energy Reviews, 2010. **14**(2): p. 754-762.
2. Gong, J., J. Liang, and K. Sumathy, *Review on dye-sensitized solar cells (DSSCs): Fundamental concepts and novel materials.* Renewable and Sustainable Energy Reviews, 2012. **16**(8): p. 5848-5860.
3. Choudhury, M.S.H., N. Kishi, and T. Soga, *Compression of ZnO nanoparticle films at elevated temperature for flexible dye-sensitized solar cells.* Journal of Alloys and Compounds, 2016. **656**: p. 476-480.
4. Saurdi, I., Shafura, AK, Azhar, NEA, Ishak, A, Malek, MF, Alrokayan, AH Salman, Khan, Haseeb A, Mamat, MH, Rusop, M, Mahmood, Mohamad Rusop. *Effect of TiO2 thickness on nanocomposited aligned ZnO nanorod/TiO2 for dye-sensitized solar cells*. in *AIP Conference Proceedings*. 2016. AIP Publishing.
5. Kang Xiaohui, J.C., Wan Zhongquan, Zhuang Jia, Feng, Juan, *A novel tri-layered photoanode of hierarchical ZnO microspheres on 1D ZnO nanowire arrays for dye-sensitized solar cells.* RSC Advances, 2015. **5**(22): p. 16678-16683.
6. Benkstein K. D., K.N., van de Lagemaat J., Frank A. J., *Influence of the Percolation Network Geometry on Electron Transport in Dye-Sensitized Titanium Dioxide Solar Cells.* The Journal of Physical Chemistry B, 2003. **107**(31): p. 7759-7767.
7. Suriati Suhaimi, M.M.S., Z.A. Alahmed, J. Chyský ,A. H. Reshak *Materials for Enhanced Dye-sensitized Solar Cell Performance: Electrochemical Application.* Int. J. Electrochem. Sci., 2015. **10**: p. 2859 - 2871.
8. J. Elias, M.B., I. Utke, R. Erni, D. Hosseini, J. Michler, L. Philippe, *Urchin-inspired zinc oxide as building blocks for nanostructured solar cells.* Nano Energy, 2012. **1**: p. 696–705.
9. Jamil Elias, C.L.v.-C.m., Mikhael Bechelany, Johann Michler, Guillaume-Yangshu Wang, Zhao Wang, and Laetitia Philippe, *Hollow Urchin-like ZnO thin Films by Electrochemical Deposition.* Adv. Mater., 2010. **22**: p. 1607–1612.
10. Matt Law, L.E.G., Aleksandra Radenovic,Tevye Kuykendall, Jan Liphardt, and Peidong Yang*, *ZnO-Al2O3 and ZnO-TiO2 Core-Shell Nanowire Dye-Sensitized Solar Cells.* J. Phys. Chem. B, 2006. **110**: p. 22652-22663.
11. Hiralal Pritesh, C.C., Lal Niraj N, Abeygunasekara Waranatha, Kumar Abhishek, Butt Haider, Zhou Hang, Unalan Husnu Emrah, Baumberg Jeremy J, Amaratunga, Gehan AJ, *Nanowire-based multifunctional antireflection coatings for solar cells.* Nanoscale, 2014. **6**(23): p. 14555-14562.
12. Zaier A., O.E.a.F., Lakfif F., Kabir A., Boudjadar S., Aida M. S., *Effects of the substrate temperature and solution molarity on the structural opto-electric properties of ZnO thin films deposited by spray pyrolysis.* Materials Science in Semiconductor Processing, 2009. **12**(6): p. 207-211.
13. Baxter, J.B. and E.S. Aydil, *Nanowire-based dye-sensitized solar cells.* Applied Physics Letters, 2005. **86**(5): p. 053114.
14. Guillen Elena, A.E., Peter Laurence M., Zukal Arnost, Tena-Zaera Ramon, Anta Juan A., *ZnO solar cells with an indoline sensitizer: a comparison between nanoparticulate films and electrodeposited nanowire arrays.* Energy & Environmental Science, 2011. **4**(9): p. 3400-3407.
15. M. Law, L.E.G., J. C. Johnson, R. Saykally, and P. Yang, *Nanowire dye-sensitized solar cells.* Nature Materials, 2005. **4**(6): p. 455–459.
16. Elias J., U.I., Yoon S., Bechelany M., Weidenkaff A., Michler J., Philippe L., *Electrochemical growth of ZnO nanowires on atomic layer deposition coated polystyrene sphere templates.* Electrochimica Acta, 2013. **110**: p. 387-392.

17. Thomas, M.A.C., Jingbiao, *Electrodeposition of ZnO nanostructures: growth, doping, and physical properties.* Handbook of Nanoelectrochemistry: Electrochemical Synthesis Methods, Properties, and Characterization Techniques, 2016: p. 647-679.
18. Zhang, Y., Guerra-Nuñez Carlos, Utke Ivo, Michler Johann, Rossell Marta D, Erni Rolf, *Understanding and Controlling Nucleation and Growth of TiO2 Deposited on Multiwalled Carbon Nanotubes by Atomic Layer Deposition.* The Journal of Physical Chemistry C, 2015. **119**(6): p. 3379-3387.
19. Guerra-Nuñez Carlos, Z.Y., Li Meng, Chawla Vipin, Erni Rolf, Michler Johann, Park Hyung Gyu, Utke Ivo, *Morphology and crystallinity control of ultrathin TiO 2 layers deposited on carbon nanotubes by temperature-step atomic layer deposition.* Nanoscale, 2015. **7**(24): p. 10622-10633.
20. J. A. van Delft, D.G.-A., W. M. M. Kessels, *Atomic layer deposition for photovoltaics: applications and prospects for solar cell manufacturing.* Semiconductor Science and Technology, 2012. **27**(7): p. 074002.
21. Marichy Catherine, B.M., Pinna Nicola, *Atomic Layer Deposition of Nanostructured Materials for Energy and Environmental Applications.* Advanced Materials, 2012. **24**(8): p. 1017-1032.
22. Bandaranayake, K.M.P.S., M. K. I.; Weligamuwa, P. M. G. M. P.; Tennakone, K., Coord. Chem. ReV., 2004. **248**: p. 1277.
23. Kirthi Tennakone, J.B., Priyangi Konara Mudiyanselage, Bandaranayake, Gamaralalage Rajanya Asoka, Kumara, Akinori, Konno, *Enhanced Efficiency of a Dye-Sensitized Solar Cell Made from MgO-Coated Nanocrystalline SnO 2.* Japanese Journal of Applied Physics, 2001. **40**(7B): p. L732.
24. Palomares Emilio, C.J.N., Haque, Saif A., Lutz Thierry, Durrant James R., *Control of Charge Recombination Dynamics in Dye Sensitized Solar Cells by the Use of Conformally Deposited Metal Oxide Blocking Layers.* Journal of the American Chemical Society, 2003. **125**(2): p. 475-482.
25. Yishay Diamant, S.C., S.G. Chen, Ophira Melamed, Arie Zaban, *Core–shell nanoporous electrode for dye sensitized solar cells: the effect of shell characteristics on the electronic properties of the electrode.* Coordination Chemistry Reviews, 2004. **248**: p. 1271–1276.
26. Yishay Diamant, S.G.C., Ophira Melamed, and Arie Zaban*, *Core-Shell Nanoporous Electrode for Dye Sensitized Solar Cells: the Effect of the SrTiO3 Shell on the Electronic Properties of the TiO2 Core.* J. Phys. Chem. B, 2003. **107**: p. 1977-1981.
27. Zaban A., C.S.G., Chappel S., Gregg B. A., *Bilayer nanoporous electrodes for dye sensitized solar cells.* Chemical Communications, 2000(22): p. 2231-2232.
28. Saxena, V. and D.K. Aswal, *Surface modifications of photoanodes in dye sensitized solar cells: enhanced light harvesting and reduced recombination.* Semiconductor Science and Technology, 2015. **30**(6): p. 064005.
29. Greene, L.E., *Next-generation photovoltaics using solution-grown zinc oxide nanowire arrays*. 2007: ProQuest.
30. Marimuthu T., A.N., Thangamuthu R., Mummoorthi M., Ravi G., *Synthesis of ZnO nanowire arrays on ZnOTiO2 mixed oxide seed layer for dye sensitized solar cell applications.* Journal of Alloys and Compounds, 2016. **677**: p. 211-218.
31. Rahman M. Y. A., R.L., Umar A. A., Salleh M. M., *Effect of boric acid composition on the properties of ZnO thin film nanotubes and the performance of dye-sensitized solar cell (DSSC).* Journal of Alloys and Compounds, 2015. **648**: p. 86-91.
32. Sobuś Jan, B.G., Karolczak Jerzy, Idígoras Jesús, Anta Juan A., Ziółek Marcin, *Comparison of TiO2 and ZnO Solar Cells Sensitized with an Indoline Dye: Time-Resolved Laser Spectroscopy Studies of Partial Charge Separation Processes.* Langmuir, 2014. **30**(9): p. 2505-2512.
33. Elias, J., R. Tena-Zaera, and C. Lévy-Clément, *Electrodeposition of ZnO nanowires with controlled dimensions for photovoltaic applications: Role of buffer layer.* Thin Solid Films, 2007. **<HT>515</HT>**(24): p. 8553-8557.

34. Peulon, S. and D. Lincot, *Cathodic electrodeposition from aqueous solution of dense or open-structured zinc oxide films.* Advanced Materials, 1996. **8**(2): p. 166-170.
35. R.Tena-Zaera, J.E., G.Wang, C.Levy-Clement, Journal of Physical Chemistry C 2007. **111**: p. 16706.
36. Li Luping, X.C., Zhao Yang, Chen Shikai, Ziegler Kirk J, *Improving performance via blocking layers in dye-sensitized solar cells based on nanowire photoanodes.* ACS applied materials & interfaces, 2015. **7**(23): p. 12824-12831.
37. Chandiran, A.K., et al., *Sub-nanometer conformal TiO(2) blocking layer for high efficiency solid-state perovskite absorber solar cells.* Advanced Materials, 2014. **26**(25): p. 4309-12.
38. Qi Junjie, L.W., Biswas Chandan Zhang, Guangjie, Sun Lifang, Wang Zengze, Hu Xiaofeng, Zhang Yue, *Enhanced power conversion efficiency of CdS quantum dot sensitized solar cells with ZnO nanowire arrays as the photoanodes.* Optics Communications, 2015. **349**: p. 198-202.
39. Ball, J.M., Lee, Michael M., Hey, Andrew, Snaith, Henry J., *Low-temperature processed meso-superstructured to thin-film perovskite solar cells.* Energy & Environmental Science, 2013. **6**(6): p. 1739-1743.
40. Liu, M., M.B. Johnston, and H.J. Snaith, *Efficient planar heterojunction perovskite solar cells by vapour deposition.* Nature, 2013. **501**(7467): p. 395-398.